Accepted Manuscript

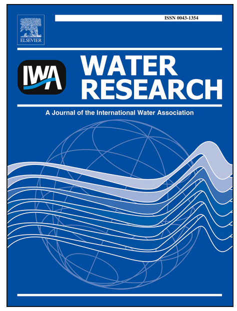

Settling characteristics of nonspherical porous sludge flocs with nonhomogeneous mass distribution

Yan Cui, Jure Ravnik, Paul Steinmann, Matjaž Hriberšek

PII: S0043-1354(19)30325-2

DOI: https://doi.org/10.1016/j.watres.2019.04.017

Reference: WR 14603

To appear in: *Water Research*

Received Date: 5 December 2018

Revised Date: 8 April 2019

Accepted Date: 9 April 2019

Please cite this article as: Cui, Y., Ravnik, J., Steinmann, P., Hriberšek, Matjaž., Settling characteristics of nonspherical porous sludge flocs with nonhomogeneous mass distribution, *Water Research* (2019), doi: https://doi.org/10.1016/j.watres.2019.04.017.

Settling characteristics of nonspherical porous sludge flocs with nonhomogeneous mass distribution

Yan Cui[a], Jure Ravnik[b], Paul Steinmann[a], Matjaž Hriberšek[b,*]

[a]*Chair of Applied Mechanics, Friedrich-Alexander Universität Erlangen-Nürnberg, Paul-Gordan-Str. 3, D-91052 Erlangen, Germany*
[b]*Faculty of Mechanical Engineering, University of Maribor, Smetanova 17, SI-2000, Maribor, Slovenia*

Abstract

The paper reports on the development of an advanced Lagrangian particle tracking model of sludge flocs that takes into account its nonspherical shape, the internal porosity and permeability, as well as the nonhomogenous mass distribution. The floc shapes, sizes and free settling velocities are determined based on the experimental measurement of settling sludge flocs originating from a wastewater treatment plant. Based on the floc shape characterization, a prolate axisymmetric ellipsoid is selected as the modelled sludge particle. In order to determine the main particle characteristics, e.g. the internal porosity, the density and the flow permeability, a Lagrangian particle tracking model is developed based on Brenner's drag model for a prolate axisymmetric ellipsoid and a buoyancy force model for a porous particle. The model is implemented for numerical simulations of the free settling process. The obtained floc characteristics are presented in the form of a two-part polynomial fitting curve, which can be used

*Corresponding author
Email addresses: yan.cui@fau.de (Yan Cui), jure.ravnik@um.si (Jure Ravnik), paul.steinmann@fau.de (Paul Steinmann), matjaz.hribersek@um.si (Matjaž Hriberšek)

to model floc characteristics. The values of settling velocities of flocs computed by the model show very good agreement with experimental results. Futhermore, as the internal structure of a floc is seldom uniform, the nonhomogeneous mass distribution is considered, influencing the rotational and translational motions of the settling flocs. The nonhomogeneous mass distribution is introduced into the floc settling model. The parametric analyses of different barycentre offsets and shear rates are performed, and their influences on the free settling velocity are evaluated. The presented modeling approach can also be applied to flocculent settling of alum and other flocs in drinking water treatment plants. The developed Lagrangian model is suitable for use as a point source within the framework of Eulerian flow computations, and is solved as a two-phase flow model with a suitable Computational Fluid Dynamics code.

Keywords: activated sludge, floc settling velocity, prolate spheroidal floc, non-homogenous porous floc, Lagrangian particle tracking model

1. Introduction

In a wastewater treatment plant the final stage consists of the sedimentation process performed in a sedimentation tank (Droste & Gehr, 2019). Due to the intense mixing in the aerobic phase of the plant operation, the sludge flocs are predominantly well distributed within the volume of the liquid phase entering the sedimentation tank. After entering, the sedimentation starts in the settling zone, where the process is characterised by the unhindered settling of the sludge flocs, i.e. without interaction with other flocs, in a dilute liquid-particle flow regime. The flocs then accumulate in the sludge zone, where the sludge floc concentration increases and particle-particle interactions start to influence the settling velocities of the flocs, with intermediate and dense liquid-particle flow regimes (Crowe et al., 2011). In general, the sludge flocs having a settling velocity larger than the critical particle are removed from the liquid entering the outlet zone of the sedimentation tank. As the settling behaviour of the flocs is influenced by the floc's physical properties and its interaction with the liquid flow, it is extremely important to determine these parameters correctly.

The sedimentation velocity of a floc is influenced significantly by its diameter and density, as predicted by the Stokes settling model, but can also depend on the floc shape and porous internal structure, as flocs are agglomerates of many primary particles (Vahedi & Gorczyca, 2014). The floc properties determine the magnitude of interaction forces with the liquid phase, where the drag force and the buoyancy force are the most important contributions. Determination of the floc properties is frequently done by using a combined experimental and computational approach, where the experiments provide information on the floc sizes and settling velocities in a free settling environment, while computational models serve as the basis for calculation of hydrodynamic properties, as well as the floc densities.

Since the sludge particles are typically smaller than the smallest flow structures, the point particle approximation can be used when developing computational sedimentation models (Crowe et al., 2011). The majority of computational force models assume a spherical floc shape, which, thus, hydrodynamically, is also the most studied one. The sphere models can be extended to nonspherical shapes by introducing a shape factor, e.g. the sphericity of a particle (Hölzer & Sommerfeld, 2009; Mando & Rosendahl, 2010). While such an approach is easy to implement and can lead to simple to use computational models for the point particle approximation (Zastawny et al., 2012), it does not provide much improvement in terms of a more detailed particle-fluid flow interaction model. As the floc shape is a result of an agglomeration process in the active phase of the wastewater treatment, its volume is composed of numerous smaller primary particles, forming a larger porous volume, consisting of primary particles and the fluid. Due to the porous structure, the fluid can penetrate, and the flow through the floc alters the floc hydrodynamic properties (Hsu & Hsieh, 2003). In order to establish a computationally lean model, the porosity and the permeability of flocs are applied further in the floc forces and properties models. Furthermore, a floc force model that takes into account more details of the floc shape can further improve the accuracy of sludge floc-fluid flow interaction models.

The use of advanced computational techniques in the modelling of activated sludge systems is still one of the major challenges in the Wastewater sector, and the use of Computational Fluid Dynamics (CFD) to model different stages in activated sludge systems is becoming one of the most advanced wastewater engineering tools (Karpinska & Bridgeman, 2016). The CFD tool must incorporate a multiphase flow model, where the building blocks are either a Eulerian or a Lagrangian two-phase flow model (Karpinska & Bridgeman, 2016; Xu et al., 2017; Gao & Stenstrom, 2018). With regard to the secondary settling, which is one of the most sensitive processes in activated sludge plants, the Lagrangian model is the most accurate option for numerical simulation of floc trajectories. As the dimensions of a typical settling tank are very large and the corresponding computational grid for the CFD typically consists of elements much larger than the size of a sludge floc, the point particle approximation, in combination with the Lagrangian particle tracking, provides an accurate computational tool for studying such systems. Also, detailed flow field computations by implementing the Large Eddy Simulations (LES) (Al-Sammarraee et al., 2009) showed that the smaller particles, (typically below $250\mu m$), are the critical ones, with the tendency to exit the system with the effluent, a consequence of long sedimentation times, influenced by the turbulent regions at the inflow and outflow of a sedimentation basin. When dealing with nonspherical particles, tracking the orientation of a nonspherical particle in a flow field is an important aspect of an accurate two-phase flow computational model, as it determines the orientation of the force vector acting on the particle (Gunes et al., 2008). The orientation is influenced by the particle shape and porous structure (Masoud et al., 2013), but could also be influenced by a nonhomogeneous mass distribution within the particle, producing an additional gravitational torque acting on the particle (Croze et al., 2013). In the case of sludge flocs, since the floc agglomeration process is a stochastic one, a nonhomogeneous mass distribution is likely to occur (Vahedi & Gorczyca, 2014). Although the majority of CFD codes include such two-phase models, the particle force models available are only applicable to solid spheres. In recent years, a lot of research was devoted to the development and implementation of nonspherical particle two-phase CFD models (Zhang et al., 2001; Mortensen et al., 2008; Soldati & Marchioli, 2009; Liu et al., 2009; Marchioli et al., 2010), where the ellipsoidal shape was used predominantly as a generic shape, applicable to a wide range of practical two-phase problems (Mando & Rosendahl, 2010; Kleinstreuer & Feng, 2013).

The Lagrangian model, in its simplified form, is also the model of choice when determination of the floc properties based on experimental sedimentation studies is performed, as reported in the experimental analysis of sludge floc sedimentation characteristics (Žajdela et al., 2008), and the consequent determination of the floc properties based on the free settling model of porous and permeable sludge flocs (Lee et al., 1996; Hriberšek et al., 2011). In order to account for the nonspherical floc shape and its porous internal structure that influences its hydraulic resistance in the flow field, a dedicated Lagrangian particle model for the sludge floc case could prove beneficial in increasing the accuracy of dispersed two-phase flow CFD computational models, especially if it would also be applicable as a computational framework for the derivation of sludge floc properties based on experimental sedimentation data. The present work reports on the development of such a model.

The paper is organised as follows. Section 2 describes the key sedimentation characteristics of sludge flocs, followed by Section 3 where the development of a Lagrangian computational sedimentation model is elaborated. Based on the developed Lagrangian model two computational algorithms are proposed, the first one suitable for use as a computational tool for the determination of floc porosities and corresponding parameters, and the second one for studying the effects of nonhomogeneous mass distribution on the sludge floc sedimentation dynamics. Section 5 reports on the results of the implementation of both computational algorithms, which are based on available experimental data on 306 sludge flocs originating from a municipal wastewater plant in Slovenia. Section 6 compares the performance of the developed models with several established hard sphere models, to understand what and how much is improved by the present model by comparing it with other models.

2. Sedimentation characteristics of activated sludge flocs

Activated sludge flocs are formed as aggregates of suspended solids, micro flocs and primary particles in wastewater, and, as such, they are not solid bodies, but exhibit an open porous internal structure, allowing the fluid phase to flow through the floc. Although the complex internal structure of a floc presents a significant resistance to the fluid flow, the flow through the floc alters the flow field in the wake, effectively reducing the drag force. This, in turn, allows the floc to reach higher settling velocities, as in the case of solid particles of the same shape, size and density.

The free settling test is used frequently for the determination of the porous particle density, porosity and hydraulic permeability, which is done through a simple force balance equation. In Žajdela et al. (2008), a free settling model was designed based on the Stokes model of sedimentation, where the Chien's model

(Chien, 1994) was used for the drag coefficient of irregularly shaped particles. Although the applied Chien's drag model is easy to use, with the only additional parameter being the particle sphericity (Ψ), the model could be improved for the case of a sludge floc with more detailed particle shape cases.

In general, settling velocities of porous sludge flocs are relatively low, resulting in low particle Reynolds number values. This is especially true in the case of smaller porous flocs (approx. below 1 mm), where particle Reynolds number values are below 1. In such a case, the Stokes flow regime is valid and the Stokes drag model could be applied. For the case of 306 flocs (Žajdela et al., 2008), originating from a primarily municipal wastewater plant, experimental analysis of the settling velocities was carried out, with the results of the settling velocities depicted in Fig. 1. From the same data, presented in the form of the particle Reynolds number values ($Re_k = \Psi d_k v_k/\nu$ with d_k the equivalent spherical diameter, v_k the settling velocity, and ν the fluid kinematic viscosity) in Fig. 2, it is evident that the vast majority of particles exhibited Reynolds number values lower than 1. Therefore, the Stokes drag model can be applied in the derivation of the floc sedimentation model.

A more realistic drag force model should also include the main geometric parameters of the floc shape. Whereas larger flocs have a typical fractal structure (Gorczyca & Ganczarczyk, 2002), the structure of the smaller flocs resembles more geometrically regular shapes. In the works of Žajdela et al. (2008) and Hriberšek et al. (2011), geometric analysis of stationary flocs, as well as settling flocs, led to the conclusion that the sludge flocs could be described approxi-

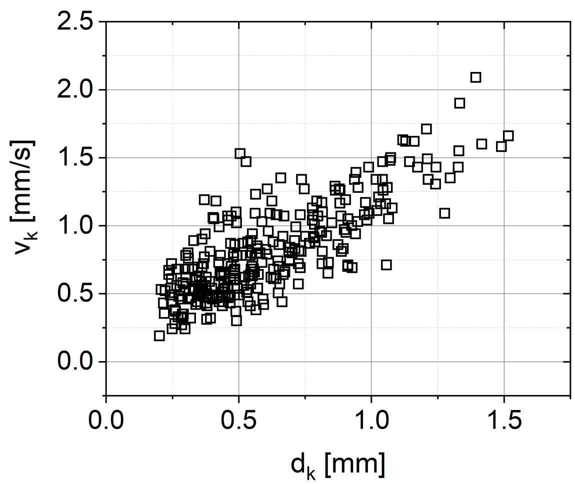

Figure 1: Experimentally measured settling velocities of sludge flocs as a function of floc diameter.

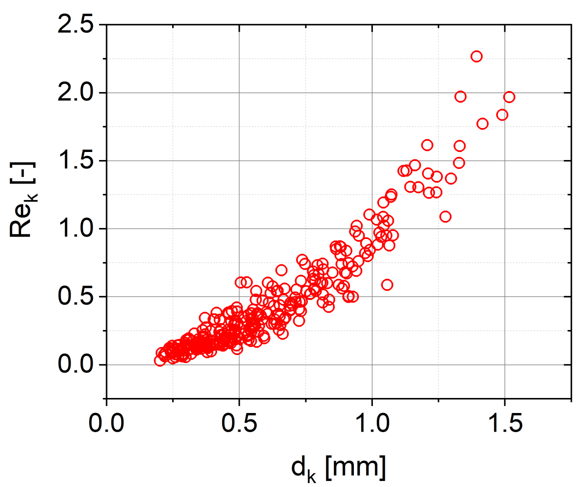

Figure 2: Experimental data on particle Reynolds number values of sludge flocs as a function of floc diameter.

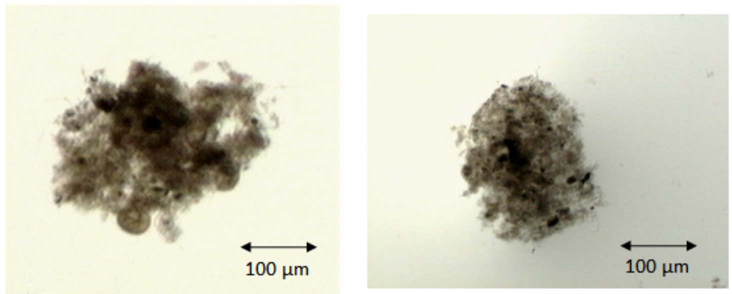

Figure 3: Shape of the studied porous flocs.

mately as cuboids, with two shorter axes of almost the same size. For the cited case, the sphericity, defined as the ratio of a sphere surface area to the surface area of a floc with the same volume, was determined to be 0.796. The cuboidal approximation could be improved further by considering the ellipsoidal shape of the studied porous flocs, as shown in Fig. 3 originating from experiments of Žajdela et al. (2008), of the same volume. The general shape of the smallest flocs could, therefore, be described as a prolate spheroid. A schematic diagram of a prolate spheroidal particle (or axisymmetric ellipsoidal particle) with semi-minor axis a and semi-major axis b, and, thus, with aspect ratio $\lambda = b/a \geq 1$, and the associated reference frame used in the computational model, are illustrated in Fig. 4. The observed axis ratio ($\lambda = b/a$) of the ellipsoids ranged between 1.29 and 1.47. For the sake of simplicity, the average value of $\lambda = 1.38$ was adopted in our case, but the sensitivity of the results on the lower and upper limit values of the aspect ratio was also checked.

Low settling velocities of sludge flocs, resulting in low values of the Stokes number, defined as $St_k = \frac{\rho_k v_k d_k}{18 \rho_f \nu}$ with ρ_f the fluid density, and in the range of

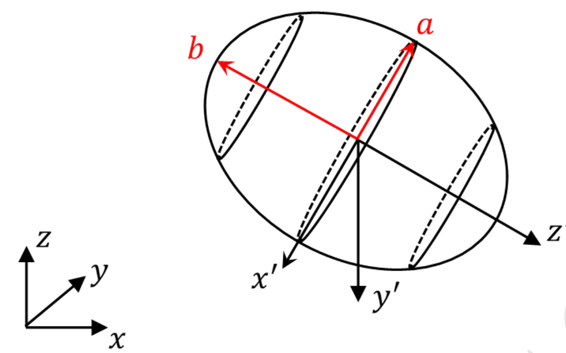

Figure 4: Schematic of a prolate spheroidal floc.

$[0.004, 0.18]$ (Hriberšek et al., 2011), also indicate that the velocity of such a particle would not differ much from the fluid flow velocity. In a settling tank, the flow field is governed by the inflow and outflow rates and positions, or, in the case of a closed system, from buoyancy driven currents, and although flow velocities in these systems are low and settling is facilitated, the particles still interact with the local fluid flow. Therefore, accurate prediction of floc trajectories could be very beneficial when designing the sedimentation process in a settling tank.

3. Computational model of ellipsoidal porous floc sedimentation

In general, the trajectory of a particle is the result of its interaction with the fluid flow. Local values of velocity, vorticity and pressure in the fluid phase and their difference to the state of the particle, determine the transport phenomena between the dispersed and the fluid phases. When the exact particle trajectories are of major importance, as is the case in sedimentation analysis, particle transport in the framework of CFD is computed by applying Lagrangian based particle tracking.

In the following, the computational model of sedimentation is derived, based on the Stokes drag model for an axisymmetric ellipsoid case (i.e. prolate spheroidal porous flocs), taking into account the translational, as well as rotational dynamics, of the floc. As the floc is ellipsoidal, its orientation regarding the flow velocity is important for the accurate computation of the hydrodynamic force, a case that is not important when dealing with the spherical approximation of the floc shape.

The sedimentation model used for the calculation of the porous floc properties can be derived from the general model of Lagrangian particle tracking, which consists of the translational kinematics relation

$$\frac{d\boldsymbol{r}}{dt} = \boldsymbol{v}, \tag{1}$$

the translational momentum conservation equation

$$m_p \frac{d\boldsymbol{v}}{dt} = \boldsymbol{F}_D + \boldsymbol{F}_G, \tag{2}$$

and the angular momentum conservation equation

$$\frac{d}{dt}\left[\boldsymbol{I}_p\,\boldsymbol{\omega}\right] = \boldsymbol{I}_p\,\frac{d\boldsymbol{\omega}}{dt} + \boldsymbol{\omega}\times\left[\boldsymbol{I}_p\,\boldsymbol{\omega}\right] = \boldsymbol{T}, \tag{3}$$

where m_p is the mass of the particle, $\boldsymbol{r}$, $\boldsymbol{v}$, $\boldsymbol{\omega}$, $\boldsymbol{I}_p$ are the barycentre position vector, the translational velocity, the angular velocity, and the inertia tensor, respectively, of the particle, and $\boldsymbol{F}_D$, $\boldsymbol{F}_G$, $\boldsymbol{T}$ are the drag force, the gravity force reduced by buoyancy, and the applied torque, respectively, acting on the particle. The angular kinematics relation is accounted for by the time evolution of the Euler parameters (Cui et al., 2018a,b). In order to close the system of equations, models for forces and torques acting on a porous floc have to be specified.

3.1. Drag and buoyancy models for prolate spheroidal porous flocs

Dedicated models of forces have to be selected in order to account for the prolate spheroidal floc shape. Brenner (1964) derived the hydrodynamic drag force acting on an axisymmetric ellipsoidal particle with semi-minor axis a in the Stokes flow regime:

$$\mathbf{F}_D = \pi a \rho_f \nu \mathbf{K}\,[\mathbf{u} - \mathbf{v}], \tag{4}$$

where $\mathbf{u}$, $\mathbf{v}$, $\mathbf{F}_D$, $\mathbf{K}$ are the corresponding coefficient matrices of the fluid velociy $\boldsymbol{u}$, the floc velocity $\boldsymbol{v}$, the drag force acting on the floc $\boldsymbol{F}_D$, and the (geometric) resistance tensor $\boldsymbol{K}$ of the floc, respectively. Only the diagonal components of the coefficient matrix of the resistance tensor in the particle frame of reference $[x', y', z']$, i.e. $\mathbf{K}'$, are non-zero; these are functions of the floc aspect ratio λ and can be written as

$$K'_{x'x'} = K'_{y'y'} = \frac{16[\lambda^2 - 1]^{3/2}}{[2\lambda^2 - 3]\ln(\lambda + \sqrt{\lambda^2 - 1}) + \lambda\sqrt{\lambda^2 - 1}} \tag{5}$$

$$K'_{z'z'} = \frac{8[\lambda^2 - 1]^{3/2}}{[2\lambda^2 - 1]\ln(\lambda + \sqrt{\lambda^2 - 1}) - \lambda\sqrt{\lambda^2 - 1}}. \tag{6}$$

The spherical particle limit renders $\lim_{\lambda \to 1} \mathbf{K}' = 6\,\mathbf{I}$, where $\mathbf{I}$ is the identity matrix. In order to build the relationship between $\mathbf{K}$ and $\mathbf{K}'$, the rotation matrix, $\mathbf{V}$, between the inertia and the particle frame of reference is used:

$$\mathbf{K} = \mathbf{V}^T \mathbf{K}' \mathbf{V}. \tag{7}$$

The rotation matrix is written in terms of the Euler parameters, and can be found in Cui et al. (2018a).

In order to account for the porosity of the floc, the ratio of the hydrodynamic drag between a permeable and an impermeable flocs, i.e. Ω, is introduced by using the Brinkman extension of Darcy's law (Huang, 1993), with Ω defined as

$$\Omega = \frac{2\beta^2 \left[1 - \tanh(\beta)/\beta\right]}{2\beta^2 + 3\left[1 - \tanh(\beta)/\beta\right]}, \tag{8}$$

with the permeability factor

$$\beta = \frac{d_k}{2\sqrt{k}}, \tag{9}$$

and the hydraulic permeability of the floc accounted for by the Brinkman model

$$k = \frac{d_p}{72}\left[3 + \frac{4}{1-\epsilon} - 3\sqrt{\frac{8}{1-\epsilon} - 3}\right], \tag{10}$$

where ϵ and d_p are the porosity of the floc and the primary particle diameter. The density of the floc ρ_k is related to the density of primary particles ρ_p, constituting the floc, and the density of the fluid ρ_f by the relation

$$\rho_k = [1 - \epsilon]\left[\rho_p - \rho_f\right] + \rho_f. \tag{11}$$

The values of $\rho_p = 1059 kg/m^3$ and $\rho_f = 998 kg/m^3$ are used in the present study (Hriberšek et al., 2011).

The final form of the drag model for the prolate spheroidal porous floc is

$$\mathbf{F}_D = \pi a \rho_f \nu \Omega \mathbf{K} [\mathbf{u} - \mathbf{v}], \tag{12}$$

and the gravity force reduced by buoyancy is

$$\mathbf{F}_G = \mathbf{g} V_p \, [1 - \epsilon] \, [\rho_p - \rho_f] \,, \tag{13}$$

where $V_p = 4\pi\lambda a^3/3$ is the volume of the prolate spheroid, $\mathbf{F}_G$ and $\mathbf{g}$ are the corresponding coefficient matrices of the gravity force reduced by buoyancy $\boldsymbol{F}_G$ and the gravity acceleration $\boldsymbol{g}$, respectively.

3.2. Sedimentation of a floc with nonhomogeneous density distribution

During the floc agglomeration process, a variety of primary particles having different sizes and also different densities aggregate into flocculi, micro flocs and, finally, floc aggregates, leading to nonhomogeneous mass distribution (Vahedi & Gorczyca, 2014). The nonhomogeneous mass distribution gives rise to gravitational torque, acting on the particle, that, additionally, influences the floc rotational dynamics and, hence, its orientation regarding the flow direction. In the following, the computational framework is described by taking into account the nonhomogenous mass distribution.

The applied torques acting on a prolate spheroidal porous floc, Eq. (3), can be decomposed into the gravitational torque $\boldsymbol{T}_G$ and Jeffery's torque $\boldsymbol{T}_J$ (Jeffery, 1922), i.e.

$$\boldsymbol{T} = \boldsymbol{T}_G + \boldsymbol{T}_J. \tag{14}$$

In order to calculate the inertia tensor and the gravitational torque, a separate computational analysis is needed in the case of a general density distribution within the particle volume. This analysis could be interpreted as a particle pre-processor, which needs to be applied before the sedimentation analysis is performed, giving as a result the barycentre location and the inertia tensor of the particle. In the analysis, the floc is decomposed into many cubic grid cells, where within a grid cell the density is assumed to be homogeneous. Therefore, the inertia tensor can be calculated by summing up the local inertia tensors for all grid cells, i.e.

$$\mathbf{I}'_p = \sum_{i=1}^{N} m_i \begin{bmatrix} y_i'^2 + z_i'^2 & -x_i' y_i' & -x_i' z_i' \\ -x_i' y_i' & z_i'^2 + x_i'^2 & -y_i' z_i' \\ -x_i' z_i' & -y_i' z_i' & x_i'^2 + y_i'^2 \end{bmatrix}, \tag{15}$$

where N is the total number of grid cells, m_i is the mass of each grid cell, x_i', y_i', z_i' are the coordinates of the centre of the i_{th} grid cell in the particle frame of reference, and $\mathbf{I}'_p$ is the coefficient matrix of the inertia tensor of the particle in the particle frame of reference.

In the case of a general density distribution within the floc, the floc volume must be discretised by a suitable number of grid cells with variable local mass values, leading to

$$\mathbf{B}'_C = \frac{\sum_{i=1}^{N} m_i \, [x_i', y_i', z_i']^T}{\sum_{i=1}^{N} m_i}, \tag{16}$$

where $\mathbf{B}'_C$ is the coefficient (column) matrix of the barycentre $\boldsymbol{B}_C$ in the particle frame of reference. Since the calculation of particle inertia tensor and barycentre position is only performed at the beginning of the simulation, it could be separated from the actual execution of computational steps of the proposed algorithms. In such a case, even at a high number of elements used for discretising

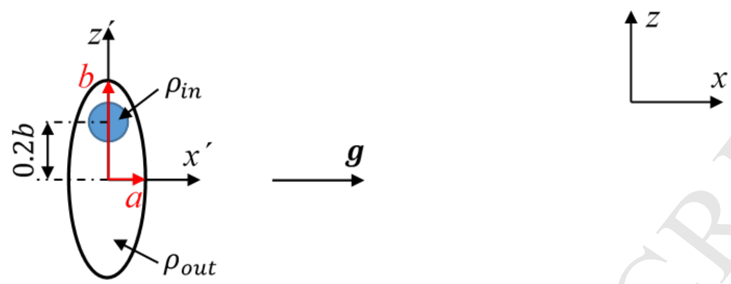

Figure 5: Schematic diagram of a particle with a two-zone density variation with its position regarding the free settling direction.

the particle interior, it would not present a considerable computational expense as these two parameters (Eqs. (15) & (16)) are calculated only once. In the present study, we use a simplied slug floc formulation, i.e. a small heavy sphere sits inside a large light prolate spheroid, as depicted in Fig. 5, in order to analyse the influence of nonhomogeneous mass distribution on the settling characteristics. In this simplied case, the analytical solution to calculate the barycenter is

$$\mathbf{B}'_C = \frac{1}{1 + \frac{\lambda a^3}{r_{in}^3}\left[\frac{\rho_{in}}{\rho_{out}} - 1\right]} \mathbf{Pos}'_{in,out}, \tag{17}$$

where r_{in} and ρ_{in} are the radius and the density of the inner spherical particle, ρ_{out} is the density of the outer prolate spheroid, and $\mathbf{Pos}'_{in,out}$ is the corresponding coefficient (column) matrix of the position vector of the inner spherical particle with respect to the geometric centre of the outer prolate spheroid at the particle frame of reference. Similarly, the coefficient matrix of the inertia

279 tensor in the particle frame of reference reads as

$$\begin{aligned}\mathbf{I}'_p &= \begin{bmatrix} \frac{1}{5}m_{out}a^2[1+\lambda^2]+\frac{2}{5}m_{in}r_{in}^2 & 0 & 0 \\ 0 & \frac{1}{5}m_{out}a^2[1+\lambda^2]+\frac{2}{5}m_{in}r_{in}^2 & 0 \\ 0 & 0 & \frac{2}{5}m_{out}a^2+\frac{2}{5}m_{in}r_{in}^2 \end{bmatrix} \\ &- m_{in}\mathbf{Pos}'_{in,out}\mathbf{Pos}'^{\,T}_{in,out}, \end{aligned} \tag{18}$$

280 with $m_{in} = 4\pi r_{in}^3[\rho_{in} - \rho_{out}]/3$ and $m_{out} = 4\pi\lambda a^3\rho_{out}/3$.

281 Finally, the gravitational torque with regard to the origin of the particle
282 frame of reference can be expressed as

$$\boldsymbol{T}_G = \boldsymbol{B}_C \times \boldsymbol{F}_G. \tag{19}$$

283 Since the Jeffery torque is defined in the particle frame of reference (Jeffery,
284 1922; Cui et al., 2018a), it is necessary to transform the coefficient (column)
285 matrix of the gravity force reduced by the buoyancy from the inertia frame of
286 reference to the particle frame of reference by using the rotation matrix $\mathbf{V}$

$$\mathbf{F}'_G = \mathbf{V}\,\mathbf{F}_G, \tag{20}$$

287 where $\mathbf{F}_G$ and $\mathbf{F}'_G$ are the coefficient (column) matrices of the gravity force,
288 reduced by the buoyancy in the inertia frame of reference and in the particle
289 frame of reference, respectively.

290 4. Computational algorithms for the determination of sludge floc 291 characteristics

292 *Algorithm 1* summarizes the computational steps needed for the determi-
293 nation of the unknown floc parameters ϵ, ρ_k, k and Ω. As the latter three all

depend on the porosity value, we are basically dealing with a nonlinear system of equations for the unknown porosity of the floc, which can be solved by using an iterative method.

In our case, derivation of the sludge floc porosity is based on the known free settling velocities of flocs of different sizes (see Fig. 1), as well as on the pre-defined floc orientation, which is the orientation of the maximum drag force where the floc has its major axis b pointing in the z-direction, i.e. perpendicular to the settling velocity direction. This orientation is chosen according to findings of Feng et al. (1994) and Ardekani et al. (2016), who showed that a spheroidal particle eventually falls with its major axis perpendicular to the gravity direction independent of its initial orientation.

Algorithm 1.

1. Set Eq. (2) for the case of terminal velocity: $d\boldsymbol{v}/dt = \mathbf{0}$.
2. Read the free settling velocity $\boldsymbol{v}_s$ and the floc equivalent circular diameter d_k from the database (Hriberšek et al., 2011), set $\boldsymbol{v} = \boldsymbol{v}_s$. Calculate the prolate spheroid short axis as $a = d_k/(2\sqrt[3]{\lambda})$.
3. Set the initial guess for the porosity value: $\epsilon = \epsilon_0$.
4. Calculate the drag model for the prolate spheroid (12) with:
   (a) Brinkman model of hydraulic permeability, Eq. (10).
   (b) The permeability factor, Eq. (9).
   (c) Ω, Eq. (8).
5. From the gravity force expression (13) calculate the updated value of porosity ϵ_{up}.

6. Check for convergence: If $[\epsilon_{up} - \epsilon]/\epsilon > 10^{-3}$ perform another iteration - go to Step 4.

7. Store the established floc parameters: ϵ, ρ_k, k and Ω.

Algorithm 1 is directly applicable to flocs with homogeneous mass distribution, which is also the assumption used in the free settling experiment of Hriberšek et al. (2011).

In order to determine the impact of the nonhomogeneous mass distribution on the floc settling characteristics, additional computational cases were performed with nonhomogeneous mass distribution. To simplify the mass distribution description, a model with two homogeneous zones of different densities was set up. The smaller inner zone has a higher density than the surrounding larger zone. As shown in Fig. 5, the inner zone locates in the $+z'$ axis of the ellipsoid. The distance between the inner zone centre and the ellipsoid centre is $0.2b$. The inner zone radius is half of the ellipsoid short radius, i.e. $0.5a$. If the density ratio $\rho_{in}/\rho_{out} = 1$, the floc has a homogeneous density distribution. If $\rho_{in}/\rho_{out} > 1$, the floc has a nonhomogeneous density distribution. It is important to note that, in the latter case, the overall mass of the floc remains unchanged with regard to the homogeneous mass distribution case. Different barycentre locations of the particle can be produced by varying the density ratio. For the case of the particle in Fig. 5, the position vector of the inner spherical particle at the particle frame of reference is $\mathbf{Pos}'_{in,out} = [0, 0, 0.2b]^T$ and the $r_{in} = 0.5a$.

As mentioned above, the floc porosity values were adopted from the computational results of *Algorithm 1.* The *Algorithm 2* was designed in order to establish the sensitivity of the settling characteristics of a floc with nonhomogeneous mass distribution. The main aim of the *Algorithm 2* is to compute the time evolution of the positions and translational and rotational velocities of the prolate spheroidal porous floc, which would then serve as a basis for comparison with the sedimentation characteristics of homogeneous flocs.

Algorithm 2.

1. Set the floc properties: d_k, λ, ϵ, Ω, ρ_{in}/ρ_{out}, and the offset distance.
2. Calculate the prolate spheroid short axis as $a = d_k/(2\sqrt[3]{\lambda})$.
3. Calculate the coefficient matrix of the inertia tensor of the prolate spheroid in the particle frame of reference $\mathbf{I}'_p$.
4. Set the initial velocity of the particle.
5. Start the time marching loop.
6. Solve the following set of equations:
   (a) Translational momentum conservation, Eq. (2).
   (b) Translational kinematics relation, Eq. (1).
   (c) Angular momentum conservation, Eq. (3) and angular kinematics relation (Cui et al., 2018a).
7. Update the particle velocity, angular velocity, position and angular position.
8. End if the target time was reached.
9. Add additional time step and perform another iteration - go to Step 6.

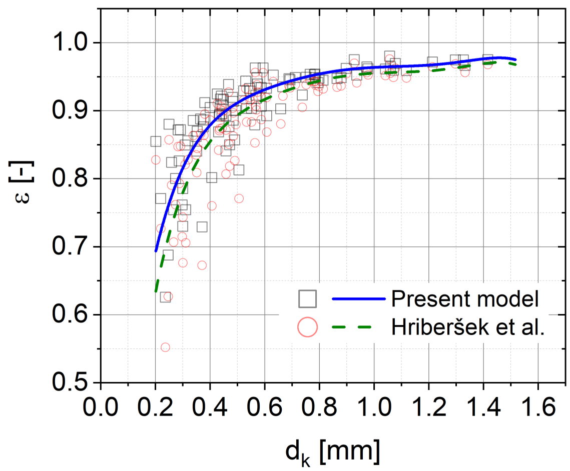

Figure 6: Porosities of sludge flocs as a function of d_k.

5. Simulation Results

5.1. Sedimentation characteristics of a floc with homogeneous density distribution

In the first part of this section, the computed porous floc porosities, obtained by applying *Algorithm 1* on all of the 306 flocs, are depicted in Fig. 6. For easier viewing, two thirds of data points in Figs. 6 - 9 were removed from the plots.

From the results, it is evident that the porosity varies in the range of 0.6 for the smallest flocs to 0.96 for the largest flocs. In order to gain additional insights and a comparison with the results of the previous study (Hriberšek et al., 2011), the calculated floc porosities are also presented as a function of the particle Reynolds number. As in the present case, the particles are porous flocs with ellipsoidal shape, the following form of the particle Reynolds number,

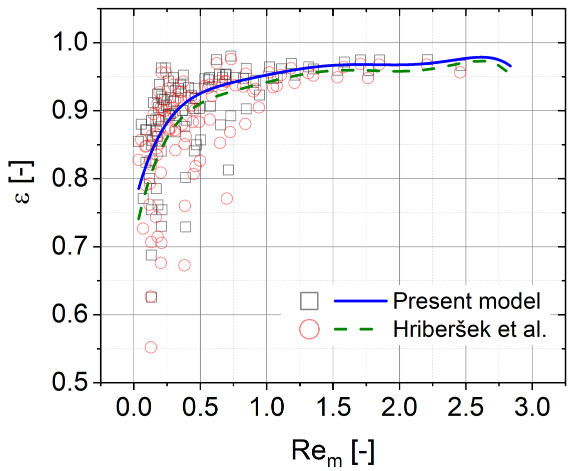

Figure 7: Porosities of sludge flocs as a function of Re_m.

374 denoted by Re_m, is used:

$$Re_m = \frac{d_k \sqrt[3]{\epsilon}\, v_k\, \Omega}{\nu} \tag{21}$$

375 From the relation between the porosity and Re_m, as shown in Fig. 7, it is evident 376 that the vast majority of flocs have Re_m values well below 1, and the maximum 377 values do not exceed 3. This indicates that the applied drag force model of 378 Brenner (1964), see Eq. (12), which is based on the same assumptions as the 379 Stokes drag, is valid for the considered case.

380 When comparing the present results with the results of Hriberšek et al. 381 (2011), as shown in Figs. 6 and 7, the results indicate, qualitatively, a good 382 agreement between both studies. However, the present results show an increase 383 in the computed porosity values, which is more evident (around 7%) in the lower 384 Re_m range than in the upper Re_m range (around 1%). This also leads to higher

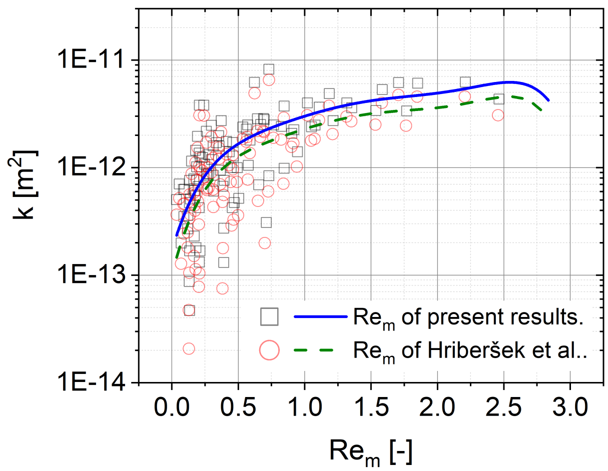

Figure 8: Permeabilities of sludge flocs as a function of Re_m.

values of computed permeabilities, as can be concluded from Fig. 8, although the permeability still remains roughly in the same order of magnitude, which is comparable to studies of other authors (Lee et al., 1996; Chu et al., 2005).

The calculated values of hydraulic permeabilities and the corresponding values of the parameter Ω (see Fig. 9) indicate the fact that the fluid flow through the floc is very weak, and, hence, the overall drag force on a floc does not differ much from the non-porous case. Nevertheless, when numerically tracking a particle/floc in a flow field for a long computational time, small differences can alter the computed trajectories significantly. Also, the obtained data on floc porosities are important, as the flocs do not only exchange momentum with the fluid, but also exchange mass due to biological reactions, where the internal surface area of a floc, which correlates with the value of the porosity, plays a

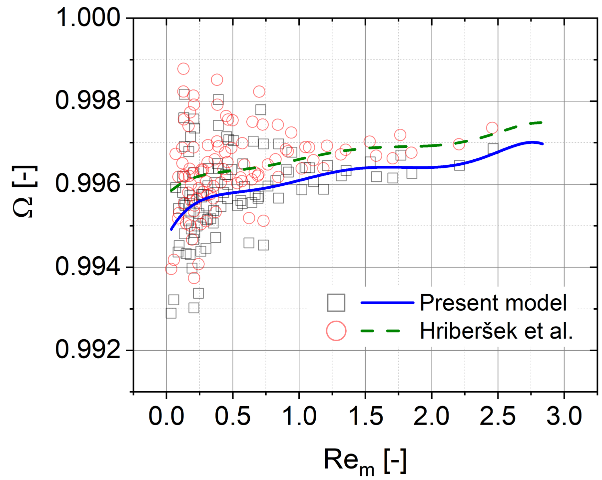

Figure 9: The ratio of the hydrodynamic drag of permeable to impermeable sludge flocs as a function of Re_m.

major role.

In order to build a model that could be used in the CFD context, a polynomial data fitting of results was performed, derived under the assumption of a homogeneous density distribution for all particles,. As is evident from the results in Fig. 6, there are two distinct dependencies of $\epsilon - d_k$, one for the larger floc equivalent diameters and the other for the smaller equivalent floc diameters, therefore, a two-part polynomial fitting was derived based on the form

$$\epsilon\,(d_k) = c_0 + c_1\,d_k + c_2\,d_k^2 + c_3\,d_k^3 + c_4\,d_k^4 + c_5\,d_k^5 + c_6\,d_k^6 \qquad (22)$$

For the range of $d_k \leq 1\,mm$ a polynomial of the 6th order, and for the range of $d_k > 1\,mm$ a polynomial of the 2th order, were fitted, with corresponding values of coefficients for all the cases listed in the Appendix, Table 2.

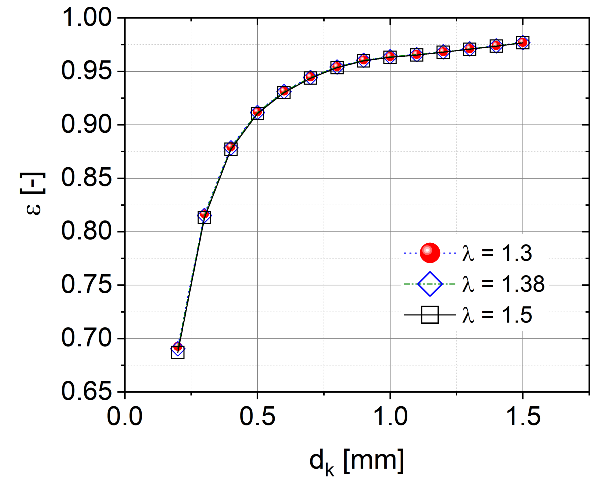

Figure 10: Impact of different aspect ratios on computational results of sludge flocs porosities.

As the application of the *Algorithm 1* was based on the assumption of a fixed ellipsoidal semi-axis ratio λ, a sensitivity study was performed of the results regarding the change of λ. Here, the lower and upper limits of the established experimental data on the floc dimensions were used, namely $\lambda = 1.3$ and $\lambda = 1.5$. Evidently, as shown in Fig. 10, the computed values of porosities for different aspect ratios of ellipsoidal flocs show that the change in the aspect ratio does not lead to different values of porosities, at least not for the targeted range of aspect ratios.

Finally, as in the derivation of the sludge floc porosity, the orientation of a floc was with its major axis b pointing in the z-direction, i.e. perpendicular to the settling velocity direction, which is the stable floc orientation with maximum flow resistance, the effect of the other significant orientation, with the long

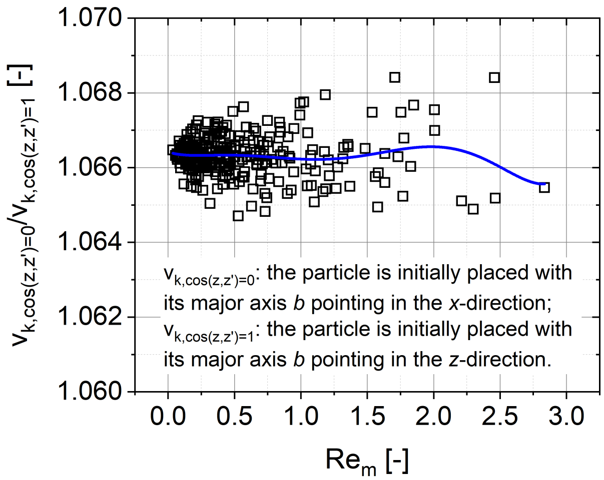

Figure 11: Ratio of settling velocities of sludge flocs with $\lambda = 1.38$ for two different initial orientations as a function of Re_m.

axis pointing in the direction of the gravity, on the sedimentation velocity was studied, with results depicted in Fig. 11. Although in all the considered floc cases (i.e. 306 flocs) each floc had its own distinct porosity value, the ratios of the computed sedimentation velocities for the two distinct orientation cases are in a very narrow range between 1.064 and 1.068. The difference of approx. 6% in sedimentation velocity between different orientations for the selected model floc with $\lambda = 1.38$ can be due to the very long retention times of several hours in a sedimentation tank, leading to a larger difference in computational results for particle trajectories with respect to spherical porous particles, and, hence, to differences in results of calculated separation efficiency of a secondary clarifier.

5.2. Sedimentation characteristics of a floc with nonhomogeneous density distribution

Nonhomogeneous mass distribution is an inherent result of the floc-forming process (Vahedi & Gorczyca, 2014), and a closer look at the different intensities of the grey areas in the porous flocs in Fig. 3 confirms this fact. As the floc images of Fig. 3 were taken using an AxioCam MRc (D) high-resolution microscopic camera offering a good spatial resolution, in the experimental sedimentation study of Hriberšek et al. (2011) a Nikon Hi Sence camera was used with a much lower resolution. It allowed estimation of the basic floc shapes, but, from these results, one could not obtain the data that could facilitate detailed infomation on the mass nonhomogeneity of each sedimenting floc. Nevertheless, in order to validate the effect of nonhomogeneous mass distribution on the sedimentation behaviour of a floc, based on available floc images, a simplified model of the floc nonhomogeneous mass distribution was given, as depicted in Fig. 5. The modelled floc consists of a dense spherical zone (ρ_{in}) and a sparse zone (ρ_{out}) of the remaining part of the floc. The distance between the centre of the dense zone and the floc geometrical centre (i.e. offset), as well as the density ratio between the dense and the sparse zones, are now the parameters which have influence on the sedimentation characteristics, as reported in this section.

With the known local mass distribution within the floc the corresponding barycentre offset and inertia tensor could be calculated easily using Eqs. (15) and (16). However, this distribution is very diffucult to determine experimentally, therefore, the following approximation was applied. As the floc formation is a stochastic process, one cannot expect that the barycentre offset should be very large, and only an estimation of this value could be made at this stage of the research. The position of the denser zone was, therefore, shifted from the centre of the ellipsoid in the z' by the distance of 20% of the longer half axis, which resulted in an additional action of the gravitational torque that would otherwise not act on the particle. With this set-up, the study of the additional gravitational torque on the particle translational and rotational dynamics could be made.

As a modelled floc, a floc was selected with $d_k = 0.29\,mm$ and the corresponding settling velocity of $v_k = 0.58\,mm/s$. The calculated porosity of the modelled floc is uniform, and has a value of $\epsilon = 0.7843$. If not reported otherwise, the default offset is $0.2b$. The application of the particle preprocessor, described in Section 3.2, gives data on the inertia tensor and on the position of the barycentre of the floc, which is shown in Fig. 12.

In all simulations, the floc was initially at rest with its major axis b pointing in the z-direction as shown in Fig. 5. In Figs. 13 and 14 the effect is presented of different density ratios on the free settling behaviour of the floc. As can be observed from Fig. 13, the shift in the barycentre and the additional gravitational torque gives rise to the floc rotation, which is stronger with increasing density ratio. The rotation changes the orientation of the floc and, hence, the drag force. The floc tends to align its long axis with the direction of the settling velocity, whereby the gravitational torque damps to zero. At this orientation angle, the

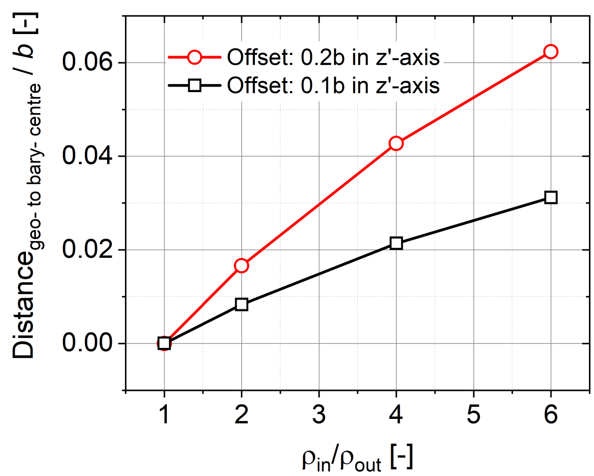

Figure 12: The relationship between the density ratio and the distance between the geometric centre and the barycentre for different offsets of inner particle centre.

frontal area of the floc is the minimum, leading to an increase of the free settling velocity (see Fig. 14), which has the same value for both nonhomogeneous test cases.

In all free settling tests, the fluid is considered at rest condition, which may violate experimental conditions, e.g. dosing of particles' buoyancy-driven natural circulation. Also, flocs that interact with the fluid flow are always exposed to locally varying fluid shear rates, giving rise to additional torque on the floc, i.e. the Jeffery torque $\boldsymbol{T}_J$ (Jeffery, 1922). In order to study the influence of the local shear rate on the floc dynamics, different linear shear rates $G = \partial u_x/\partial z$ are applied, resulting in different values of the shear Reynolds number $Re_G = d_k^2 G/\nu$. Shear rate values used in the numerical examples are typical for the sedimentation tank, see velocity profiles in Tarpagkou &

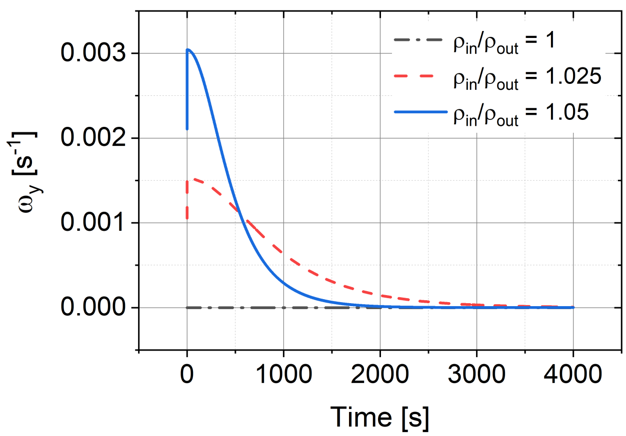

Figure 13: Time evolution of the angular velocity around y-axis of a single free-rotating sludge floc sedimented in stagnation flow field for different density ratios.

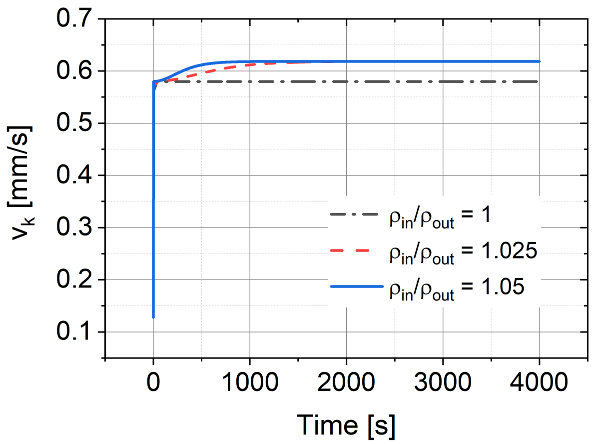

Figure 14: Time evolution of the settling velocity of a single free-rotating sludge floc sedimented in stagnation flow field for different density ratios.

Pantokratoras (2013), and range from $0.0012\,s^{-1}$ to $0.006\,s^{-1}$.

In Figs. 15 and 16 the effect of different shear rates on the free settling behaviour of the floc with $\rho_{in}/\rho_{out} = 1.05$ is presented. The action of Jeffery's torque as a consequence of the shear rate leads to much stronger interaction between the floc and the fluid, Cui et al. (2018a, 2019). The shear rate forces the floc to rotate constantly in a clockwise direction around the y-axis, while the gravitational torque acts in the clockwise or counterclockwise directions around the y-axis, depending on the signum of the cross product between the position vector of the barycentre and the direction of the gravity vector. The end effect is either almost equilibrium of both torques (case of $Re_g = 0.0001$), or a larger difference of both torques producing stronger oscillations in the rotation rate (case of $Re_g = 0.0005$). In the case of $Re_g = 0.0005$, the free settling velocity condition is never met and the tumbling motion is induced.

6. Comparison of the developed models with hard sphere models

Although sludge flocs are clearly porous objects, the hard sphere models are currently used predominantly in computational studies of sedimentation. The case of the dispersed solid phase in the form of sludge flocs is often treated as a pseudo solid phase, whose influence on the fluid flow is accounted for by introduction of the sludge viscosity, as well as additional interaction forces between the liquid and solid phases. On the other hand, Lagrangian particle tracking was applied in the CFD study of the sedimentation tank performance (Goula et al., 2008), where the particle structure effect was accounted for by the ratio

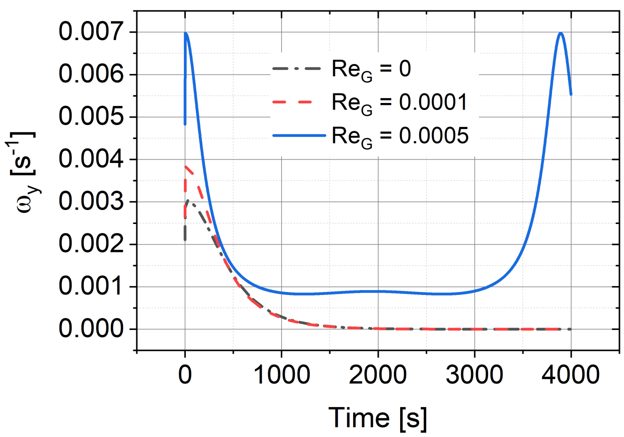

Figure 15: Time evolution of the angular velocity around y-axis of a single free-rotating sludge floc sedimented in stagnation flow field for different shear rates ($\rho_{in}/\rho_{out} = 1.05$).

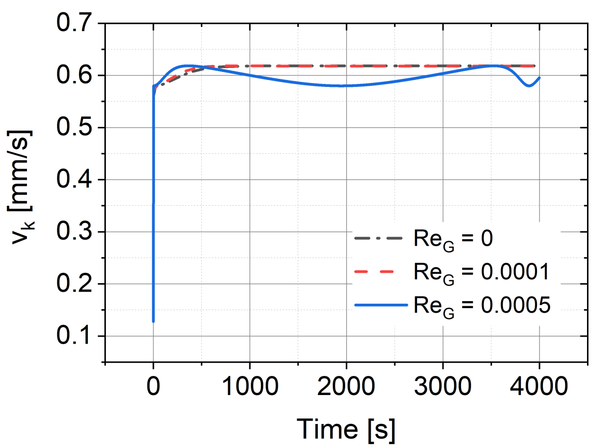

Figure 16: Time evolution of the settling velocity of a single free-rotating sludge floc sedimented in stagnation flow field for different shear rates ($\rho_{in}/\rho_{out} = 1.05$).

of the resistance experienced by a floc to that of an equivalent solid sphere (set to 0.9), and setting the apparent density at 1066 kg/m^3 regardless of the particle size. In Spelman & Sansalone (2017) a hard sphere based unsteady CFD simulation with Lagrangian particle tracking was used for computing particle sequestration, with interesting results that the simulation results showed consistently an over prediction of particles‘ sequestration compared with measured results.

Since a hydrated sludge floc is essentially a gelatinous, coagulated material (Lei & Ni, 2014), its hydrodynamic properties, that govern interaction with the liquid phase, are different than that of a solid sphere, which is a standard representation of a sludge floc. Using hard sphere models, that are available in all vendor CFD codes, inevitably leads to modelling errors, especially if the density of flocs of various sizes are set as a constant value. As an example, in Table 1 a Root Mean Square Deviation (RMSD), and its normalised form (NRMSD) are presented, produced by implementing the different models for calculation of the free settling velocity for the flocs from our experiment. Selected models include the model of Morsi & Alexander (1972) and Clift et al. (1978), which are a standard quadratic hard sphere model with Reynolds number dependent drag coefficient effectively linking the linear drag dependence with quadratic drag dependence region. The model used in Goula et al. (2008) builds on the CFD code Fluent based Stokes particle drag model by applying a fixed value of the ratio of the resistance experienced by a floc to that of an equivalent solid sphere, set at 0.9. The model of Chien (1994) is another example of a hard sphere model which additionally takes into account the sphericity of the floc. In order to amplify the need to take into account the variation of the density values of a floc with regard to its size, two additional calculations were performed, the first with a fixed floc density value of 1066 kg/m^3, and the second with the floc density value, calculated by Eq. (11), by using the porosity values of Eq. (22) (results depicted in Fig. 17). From the results, it is evident that using a constant value of floc density leads to large errors in calculating free settling velocity, especially for larger values of floc diameters. If such parameters are used in combination with standard CFD drag models in the CFD simulation to compute sludge floc trajectories, there is a danger of overestimating the separation efficiency of a tested clarifier design. When the size dependent porosity value and, consequently, the density value of the floc are used, the results are significantly better. Nevertheless, if floc permeability and shape are not taken into account (hard sphere models), the RMSD and NRMSD are still significantly larger compared with the results obtained by using the model developed in this work. This is also evident from the comparison of the model results for the variable density case, and the measured values of the velocities shown in Fig. 18. As can be observed, the hard sphere models led to increased errors with increasing floc size, even in the case of variable density, whereas the results of the present model show a very good agreement in the entire range of floc sizes.

It is not only important to have an accurate model for the calculation of the free settling velocities and, hence, an accurate prediction of the sludge floc

Table 1: Root mean square deviation (RMSD) and normalized RMSD (NRMSD) of sedimentation velocities by different models.

	Present model	Goula et al. (2008)	Clift et al. (1978)	Chien (1994)
RMSD $[m/s]$ with $\rho_k = 1066\,kg/m^3$	1.12E-05	4.41E-02	1.68E-02	2.13E-02
NRMSD $[-]$ with $\rho_k = 1066\,kg/m^3$	0.0106	41.8103	15.9533	20.1578
RMSD $[m/s]$ with ρ_k by Eq.(11)	1.12E-05	1.36E-04	8.55E-05	1.40E-04
NRMSD $[-]$ with ρ_k by Eq.(11)	0.0106	0.1287	0.0811	0.1327

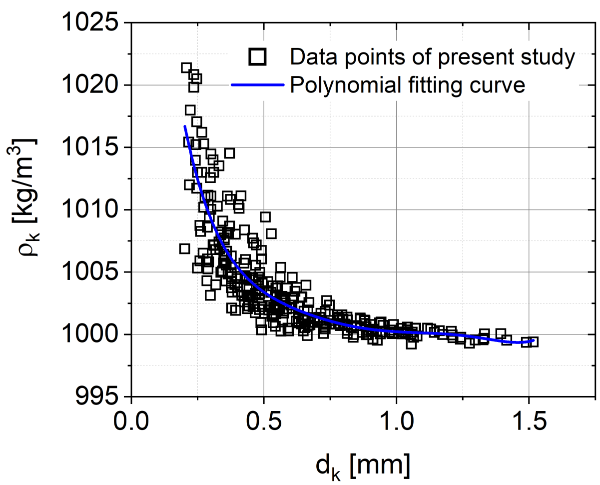

Figure 17: Sludge floc density as a function of d_k.

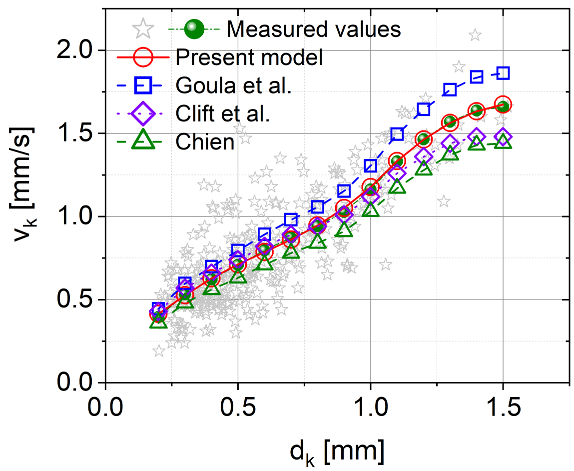

Figure 18: Comparison of calculated free settling velocities using the developed floc density vs. d_k function for different models: Goula et al. (2008), Clift et al. (1978), Chien (1994) vs. results of the present model.

trajectories. The present model can also be used instead of the hard sphere models as a model for a more accurate specification of the interaction force between the phases in the two-way coupling regime, with implementation of the models Eq. (12) and Eq. (13) as the main contributions to the interaction force in the liquid phase.

7. Discussion

The computational models developed in this work allow a direct implementation in the CFD with Lagrangian model for tracking the dispersed phase particles (sludge flocs) through the flow field of the continuous liquid phase, which is a relevant topic in sedimentation tanks' design (Tarpagkou & Pantokratoras, 2013; Al-Sammarraee et al., 2009). The sludge floc trajectories are computed evaluating the kinematics relation (1), translational momentum relation (2) as well as angular momentum relation (3), which, together with models (12), (13) and (14), allow computation of trajectories for the case of porous permeable sludge flocs of nonspherical shape. Computing particle trajectories, their rotational rates, as well as the influence of fluid velocity gradients, are important in CFD modelling of flocculation in water treatment plants (Bridgeman et al., 2009). The advanced particle tracking model can also be used in assessing the Residence Time Distribution (RTD) of the porous flocs in a sedimentation tank, allowing us to obtain RTDs for a wide range of the sludge floc parameters. Therefore, for assessing RTDs of the smaller particles that, typically, interact with the liquid phase in the dilute flow regime, the developed Lagrangian sludge floc model, together with an LES based flow simulation, would be a method of choice.

As stated in Karpinska & Bridgeman (2016) the most critical issue in modeling of clarifiers is linked to the unpredictability of activated sludge settlability, presenting a challenge for the CFD models. As the sedimentation tanks are considered as a bottle neck limiting the capacity of the wastewater treatment plant, and the CFD based design with its scale-up capabilities is becoming more and more a method of choice for the designers, one has to be careful in sedimentation modelling when using the standard particle models within the multiphase CFD codes. Within the classical solid sphere settling models, a danger of overestimating the settling velocity of flocs when floc size independent density values are used, can lead to computation of unrealistic floc trajectories, and overestimation of settling effectiveness under chosen tank operating conditions. The modeling strategy presented in this work, can help improve the accuracy of particle-fluid interaction models by considering the size dependent density, particle shape, as well as nonhomogeneous mass distribution, and can, therefore, improve the engineering design of clarifiers by means of CFD.

The presented particle models are by no means applicable only to modeling of sludge floc sedimentation processes. An interesting case arises in treatment of low-strength wastewaters in expanded sludge bed reactors (EGSB), where active biomass in the form of granules is used to reduce the polluting powers of wastewaters, (McHugh et al., 2003). In such systems, determination of settling characteristics of granules, consisting of a permeable solid part, as well as a gas phase (Pan et al., 2016), which can also lead to nonhomogeneous mass distribution, is cruical for design and operation, especially for setting the higher superficial velocities required in an EGSB reactor while still preventing the granule floatation (Chen et al., 2010). Another examples include floatation of sludge flocs in pressurised floatation tanks, where the sludge flocs merge with micro bubbles from the oversatured wastewater to form particles with possible nonhomogeneous mass distribution, and the problem of washout of floating sludge particles in Aerobic Granular Sludge reactors due to degasification of nitrogen gas (van Dijk et al., 2018). In the latter cases, the simplified nonhomogeneous mass distribution model Eqs. (17) and (18) could easily be implemented. Additionally, the presented model is by no means limited to nonhomogeneous porous particles; it can also be applied in the case of transport of bottom heavy cells like algae, that are affected by shear flow and viscous and gravitational torques (Croze et al., 2013).

One of the main limitations in practical use of the Lagrangian models is in its computational cost. As the particle dynamics is an ideally parallelizable computational step within a CFD framework, with the wide availability of desktop multiprocessor computers, the particle tracking algorithm can be run extremely efficiently in parallel, especially when used with CPU-GPU processing systems (Sweet et al., 2018). With regard to the developed models in this work, the computational cost would be roughly the same as with the standard hard sphere models if rotational dynamics would not be included, and with rotational dynamics this would then include evaluating six additional algebraic expressions for advancing the solutions of the ordinary differential equations per each particle, which is, computationally, not expensive.

8. Conclusions

One of the critical parts in the design of the settling tank in waste-water treatment is to prevent the sludge flocs from exiting the tank along with the clean liquid. A detailed determination of parameters, influencing the settling characteristics of sludge flocs, is typically achieved from data analysis from the free settling experiments. The results of such analysis can be used in a CFD-based modelling of the fluid phase and the accompanying particle tracking of the sludge flocs within the fluid flow, which can give a valuable insight into the performance of the settling tank. In this respect, the main findings are:

- The settling characteristics of sludge flocs depend on sludge floc properties, with the main influences the floc density, hydraulic permeability and shape.
- Density and permeability values of the sludge floc depend on the size of the floc, and should not be taken as constant values in computational procedures.
- The velocity of a floc in a settling process depends also on flocs' orientation, a consequence of its nonspherical shape as well as nonhomogeneous mass distribution, therefore rotational dynamics of the floc should be taken into account.
- The derived Lagrangian model is applicable both as the Lagrangian particle solver in the CFD framework and, in a simplified form, as the computational model for the determination of sludge floc porosity and related hydrodynamic properties based on data from the free settling tests.

Acknowledgement: the authors thank the Deutsche Forschungsgemeinschaft for the financial support in the framework of the project STE 544/58.

Appendix A

Table 2: Coefficients of polynomial fitting curves for different parameters.

$\epsilon\,(d_k)$	c_0	c_1	c_2	c_3	c_4	c_5	c_6
$v_{k,exp},\, d_k \leq 1\,mm$	2.86664E-04	-3.13690E-01	7.83167E+03	-1.91751E+07	2.10618E+10	-1.03534E+13	1.83831E+15
$v_{k,exp},\, d_k > 1\,mm$	-2.03000E-03	4.67862E+00	-1.47325E+03	0	0	0	0
$\lambda = 1.3$							
$\epsilon_{sim},\, d_k \leq 1\,mm$	2.87300E-02	5.58483E+03	-1.51475E+07	2.25625E+10	-1.88211E+13	8.21040E+15	-1.45401E+18
$\epsilon_{sim},\, d_k > 1\,mm$	9.47470E-01	8.38165E+00	7.58728E+03	0	0	0	0
$\Omega_{sim},\, d_k \leq 1\,mm$	9.98580E-01	-1.36895E+01	1.56698E+04	5.84723E+06	-2.23552E+10	1.55827E+13	-3.66385E+15
$\Omega_{sim},\, d_k > 1\,mm$	9.91290E-01	7.19899E+00	-2.49872E+03	0	0	0	0
$\lambda = 1.38$							
$\epsilon_{sim},\, d_k \leq 1\,mm$	2.14400E-02	5.62763E+03	-1.52652E+07	2.27393E+10	-1.89688E+13	8.27464E+15	-1.46532E+18
$\epsilon_{sim},\, d_k > 1\,mm$	9.47620E-01	7.56147E+00	7.99765E+03	0	0	0	0
$\Omega_{sim},\, d_k \leq 1\,mm$	9.98670E-01	-1.41146E+01	1.69982E+04	3.68387E+06	-2.04830E+10	1.47650E+13	-3.52216E+15
$\Omega_{sim},\, d_k > 1\,mm$	9.91280E-01	7.25300E+00	-2.52251E+03	0	0	0	0
$\lambda = 1.5$							
$\epsilon_{sim},\, d_k \leq 1\,mm$	1.06800E-02	5.68866E+03	-1.54291E+07	2.29816E+10	-1.91702E+13	8.36239E+15	-1.48087E+18
$\epsilon_{sim},\, d_k > 1\,mm$	9.46610E-01	8.34869E+00	7.80724E+03	0	0	0	0
$\Omega_{sim},\, d_k \leq 1\,mm$	9.98750E-01	-1.43650E+01	1.75976E+04	2.86071E+06	-1.98400E+10	1.44907E+13	-3.47189E+15
$\Omega_{sim},\, d_k > 1\,mm$	9.91390E-01	7.12173E+00	-2.47449E+03	0	0	0	0

652 **Appendix B**

Notation:. *Tensors* of various order are expressed in bold italic font, i.e. a first-order tensor (vector) and a second-order tensor are denoted by $\boldsymbol{A}$ and $\boldsymbol{B}$, respectively. In a Cartesian coordinate system with base vectors $\boldsymbol{e}_i$ ($i = x, y, z$) they have the coordinate representation $\boldsymbol{A} = A_i \boldsymbol{e}_i$ and $\boldsymbol{B} = B_{ij} \boldsymbol{e}_i \otimes \boldsymbol{e}_j$, respectively, whereby Einstein's summation convention applies for repeated indices. A_i and B_{ij} are the *coefficients* of $\boldsymbol{A}$ and $\boldsymbol{B}$, respectively, in the chosen coordinate system $\boldsymbol{e}_i$. They may be arranged into *coefficient matrices*

$$\mathbf{A} := \begin{bmatrix} A_x \\ A_y \\ A_z \end{bmatrix} \quad \text{and} \quad \mathbf{B} := \begin{bmatrix} B_{xx} & B_{xy} & B_{xz} \\ B_{yx} & B_{yy} & B_{yz} \\ B_{zx} & B_{zy} & B_{zz} \end{bmatrix}$$

whereby bold non-italic font is used for coefficient matrices. Indeed $\mathbf{A}$ is a column matrix, the superscript T denotes transposition so that $\mathbf{A}^T = [A_x, A_y, A_z]$ (a row matrix). Futhermore, we restrict ourselves to the use of (local) Cartesian coordinate systems $\boldsymbol{e}_i$ and $\boldsymbol{e}'_i$ that are related via rotation with rotation matrix $\mathbf{V}$ (or likewise by rotation tensor $\boldsymbol{Q}$), i.e.

$$\boldsymbol{e}'_i = V_{ik}\boldsymbol{e}_k = [V_{lk}\boldsymbol{e}_k \otimes \boldsymbol{e}_l] \cdot \boldsymbol{e}_i =: \boldsymbol{Q} \cdot \boldsymbol{e}_i \quad \text{with} \quad \mathbf{Q} = \mathbf{V}^T.$$

Without loss of generality we will thus only use the corresponding matrix arrangements of tensor coefficients, whereby upon rotation of the coordinate system $\boldsymbol{e}_i$, the corresponding coefficient matrices transform as

$$\mathbf{A}' = \mathbf{V}\,\mathbf{A} \quad \text{and} \quad \mathbf{B}' = \mathbf{V}\,\mathbf{B}\,\mathbf{V}^T.$$

References

Al-Sammarraee, M., Chan, A., Salim, S., & Mahabaleswar, U. (2009). Large-eddy simulations of particle sedimentation in a longitudinal sedimentation basin of a water treatment plant. part i: Particle settling performance. *Chemical Engineering Journal*, *152*, 307–314. doi:doi:10.1016/j.cej.2009.04.062.

Ardekani, M. N., Costa, P., Breugem, W. P., & Brandt, L. (2016). Numerical study of the sedimentation of spheroidal particles. *International Journal of Multiphase Flow*, *87*, 16–34.

Brenner, H. (1964). The Stokes resistance of an arbitrary particle - IV. Arbitrary fields of flow. *Chem. Eng. Sci*, *19*, 703–727.

Bridgeman, J., Jefferson, B., & Parsons, S. A. (2009). Computational fluid dynamics modelling of flocculation in water treatment: A review. *Engineering Applications of Computational Fluid Mechanics*, *3*, 220–241.

Chen, J., Ji, Q., Zheng, P., Chen, T., Wang, C., & Mahmood, Q. (2010). Floatation and control of granular sludge in a high-rate anammox reactor. *Water Research*, *44*, 3321–3328.

Chien, S. F. (1994). Settling velocity of irregularly shaped particles. *SPE Drilling and Completion*, (pp. 281–289).

Chu, C., Lee, D., & Tay, J. (2005). Floc model and intrafloc flow. *Chem. Engng. Sci*, *60*, 565–575.

Clift, R., Grace, J., & Weber, M. (1978). *Bubbles, Drops, and Particles*. Academic Press.

Crowe, C. T., Schwarzkopf, J. D., Sommerfeld, M., & Tsuji, Y. (2011). *Multiphase Flows with Droplets and Particles*. CRC Press.

Croze, O. A., Sardina, G., Ahmed, M., Bees, M. A., & Brandt, L. (2013). Dispersion of swimming algae in laminar and turbulent channel flows: consequences for photobioreactors. *Journal of the Royal Society Interface*, *10*.

Cui, Y., Ravnik, J., Hriberšek, M., & Steinmann, P. (2018a). A novel model for the lift force acting on a prolate spheroidal particle in an arbitrary non-uniform flow. part i. lift force due to the streamwise flow shear. *International Journal of Multiphase Flow*, *104*, 103–112. doi:10.1016/j.ijmultiphaseflow.2018.03.007.

Cui, Y., Ravnik, J., Hriberšek, M., & Steinmann, P. (2018b). On constitutive models for the momentum transfer to particles in fluid-dominated two-phase flows. In *Advanced Structured Materials* (pp. 1–25). Springer International Publishing. doi:10.1007/978-3-319-70563-7_1.

Cui, Y., Ravnik, J., Verhnjak, O., Hriberšek, M., & Steinmann, P. (2019). A novel model for the lift force acting on a prolate spheroidal particle in an arbitrary non-uniform flow. part ii. lift force taking into account the non-streamwise flow shear. *International Journal of Multiphase Flow*, *111*, 232–240. doi:10.1016/j.ijmultiphaseflow.2018.12.003.

van Dijk, E., Pronk, M., & van Loosdrecht, M. (2018). Controlling effluent suspended solids in the aerobic granular sludge process. *Water Research*, *147*, 50–59.

Droste, R. L., & Gehr, R. L. (2019). *Theory and Practice of Water and Wastewater Treatment, Second Edition.*. John Wiley & Sons Inc.

Feng, J., Hu, H., & Joseph, D. (1994). Direct simulation of initial value problems for the motion of solid bodies in a newtonian fluid part 1. sedimentation. *J. Fluid Mech*, *261*, 95–134.

Gao, H., & Stenstrom, M. (2018). Evaluation of three turbulence models in predicting the steady state hydrodynamics of a secondary sedimentation tank. *Water research*, *143*, 445–456.

Gorczyca, B., & Ganczarczyk, J. (2002). Flow rates through alum coagulation and activated sludge flocs. *Water Qual. Res. J. Canada*, *37*, 389–398.

Goula, A. M., Kostoglou, M., & Zouboulis, T. D. K. A. I. (2008). The effect of influent temperature variations in a sedimentation tank for potable water treatmentŮ a computational fluid dynamics study. *Water Research*, *42*, 3405–3414.

Gunes, D. Z., Scirocco, R., Mewis, J., & Vermant, J. (2008). Flow-induced orientation of non-spherical particles: Effect of aspect ratio and medium rheology. *J. Non-Newtonian Fluid Mech*, *155*, 39–50.

Hölzer, A., & Sommerfeld, M. (2009). Lattice boltzmann simulations to determine drag, lift and torque acting on non-spherical particles. *Computers & Fluids*, *38*, 572–589. doi:10.1016/j.compfluid.2008.06.001.

Hriberšek, M., Žajdela, B., Hribernik, A., & Zadravec, M. (2011). Experimental and numerical investigations of sedimentation of porous wastewater sludge flocs. *Water Research*, *45*, 1729–1735. doi:10.1016/j.watres.2010.11.019.

Hsu, J.-P., & Hsieh, Y.-H. (2003). Drag force on a porous, non-homogeneous spheroidal floc in a uniform flow field. *Journal of Colloid and Interface Science*, *259*, 301–308.

Huang, H. (1993). Porosity - size relationship of drilling mud flocs: fractal structure. *Clay Miner.*, *41*, 373–379.

Jeffery, G. B. (1922). The motion of ellipsoidal particles immersed in a viscous fluid. *Proceedings of the Royal Society A: Mathematical, Physical and Engineering Sciences*, *102*, 161–179. doi:10.1098/rspa.1922.0078.

Karpinska, A. M., & Bridgeman, J. (2016). Cfd-aided modelling of activated sludge systems e a critical review. *Water research*, *88*, 861–879.

Kleinstreuer, C., & Feng, Y. (2013). Computational analysis of non-spherical particle transport and deposition in shear flow with application to lung aerosol dynamics—a review. *Journal of Biomechanical Engineering*, *135*, 021008. doi:10.1115/1.4023236.

Lee, D. J., Chen, G. W., & Hsieh, C. C. (1996). On the free-settling test for estimating activated sludge floc density. *Water Research*, *30*, 541–550.

Lei, L., & Ni, J. (2014). Three-dimensional three-phase model for simulation of hydrodynamics, oxygen mass transfer, carbon oxidation, nitrification and denitrification in an oxidation ditch. *Water Research*, *53*, 200–214.

Liu, D., Keaveny, E. E., Maxey, M. R., & Karniadakis, G. E. (2009). Force-coupling method for flows with ellipsoidal particles. *Journal of Computational Physics*, *228*, 3559–3581.

Mando, M., & Rosendahl, L. (2010). On the motion of non-spherical particles at high Reynolds number. *Powder technology*, *202*, 1–13.

Marchioli, C., Fantoni, M., & Soldati, A. (2010). Orientation, distribution and deposition of elongated, inertial fibers in turbulent channel flow. *Phys. Fluids*, *49*, 33301.

Masoud, H., Stone, H. A., & Shelley, M. J. (2013). On the rotation of porous ellipsoids in simple shear fows. *J. Fluid Mech.*, *733*, R6.

McHugh, S., C., O., T., M., E., C., & V., O. (2003). Anaerobic granular sludge bioreactor technology. *Reviews in Environmental Science and Bio/Technology*, *2*, 225–245.

Morsi, S., & Alexander, A. J. (1972). An investigation of particle trajectories in two-phase flow systems. *Journal of Fluid Mechanics*, *55*, 193–208. doi:10.1017/S0022112072001806.

Mortensen, P. H., Andersson, H. I., Gillissen, J. J. J., & Boersma, B. J. (2008).

Dynamics of prolate ellipsoidal particles in a turbulent channel flow. *Physics Fluids*, *20*, 93302.

Pan, K., Su, K., Zhang, S., Sun, Z., Xu, D., & Liu, S. (2016). Hydrodynamics and permeability of aerobic granular sludge: The effect of intragranular characteristics and hydraulic conditions. *Biochemical Engineering Journal*, *113*, 133–140.

Soldati, A., & Marchioli, C. (2009). Physics and modelling of turbulent particle deposition and entrainment: Review of a systematics study. *Int. J. Multiphase Flow*, *35*, 827–839.

Spelman, D., & Sansalone, J. J. (2017). Methods to model particulate matter clarification of unit operations subject to unsteady loadings. *Water Research*, *115*, 347–359.

Sweet, J., Richter, D., & Thain, D. (2018). Gpu acceleration of eulerianŨlagrangian particle-laden turbulent flow simulations. *International Journal of Multiphase Flow*, *99*, 437–445.

Tarpagkou, R., & Pantokratoras, A. (2013). Cfd methodology for sedimentation tanks: The effect of secondary phase on fluid phase using dpm coupled calculations. *Applied Mathematical Modelling*, *37*, 3478–3494. doi:10.1016/j.apm.2012.08.011.

Vahedi, A., & Gorczyca, B. (2014). Settling velocities of multifractal flocs formed in chemical coagulation process. *Water research*, *53*, 322–328.

Xu, G., Yin, F., Xu, Y., & Yu, H.-Q. (2017). A force-based mechanistic model for describing activated sludge settling process. *Water research*, *127*, 118–126.

Žajdela, B., Hriberšek, M., B., & Hribernik, A. (2008). Experimental investigations of porosity and permeability of flocs in the suspensions of biological water treatment plants. *J. Mech. Engng.*, *54*, 547–556.

Zastawny, M., Mallouppas, G., Zhao, F., & van Wachem, B. (2012). Derivation of drag and lift force and torque coefficients for non-spherical particles in flows. *Int. J. Multiphase Flow*, *39*, 227–239.

Zhang, H., Ahmadi, G., Fan, F. G., & McLaughlin, J. B. (2001). Ellipsoidal particles transport and deposition in turbulent channel flows. *Int. J. Multiphase Flow*, *27*, 971–1009.

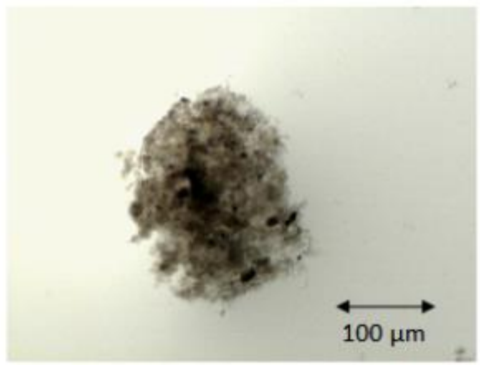

100 μm

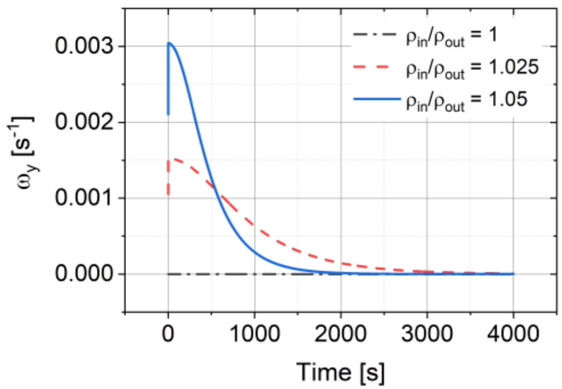

ρ_{in}/ρ_{out} = 1
ρ_{in}/ρ_{out} = 1.025
ρ_{in}/ρ_{out} = 1.05
ω_y [s^{-1}]
0.003
0.002
0.001
0.000
0
1000
2000
3000
4000
Time [s]

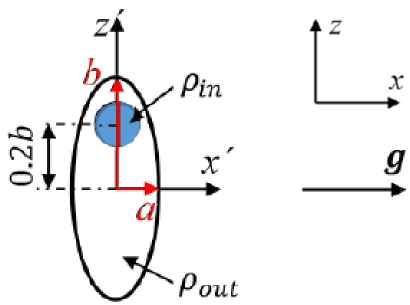

z'
b
ρ_{in}
$0.2b$
x'
a
ρ_{out}
z
x
$\boldsymbol{g}$

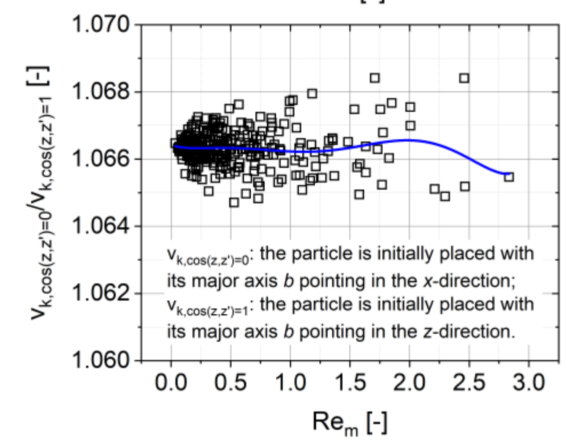

$v_{k,\cos(z,z')=0}/v_{k,\cos(z,z')=1}$ [-]
1.070
1.068
1.066
1.064
1.062
1.060
$v_{k,\cos(z,z')=0}$: the particle is initially placed with its major axis b pointing in the x-direction;
$v_{k,\cos(z,z')=1}$: the particle is initially placed with its major axis b pointing in the z-direction.
0.0
0.5
1.0
1.5
2.0
2.5
3.0
Re_m [-]

- A Lagrangian model for tracking of nonspherical porous flocs is derived.
- The floc's nonhomogeneous mass distribution is accounted for.
- The model is validated on settling characteristics of 306 wastewater porous flocs.
- The model can be applied to settling of flocs in WTP and bioreactors.
- The Lagrangian model is ready for the use in the CFD of dispersed two phase flows.